Chinese Chemical Letters 31 (2020) 1593–1597

Contents lists available at ScienceDirect

Chinese Chemical Letters

journal homepage: www.elsevier.com/locate/cclet

Communication

Aqueous-processed insulating polymer/nanocrystal solar cells with effective suppression of the leakage current and carrier recombination

Henan Sun[a,1], Nannan Chen[a,1], Yaohua Wang[a,1], Gan Jin[b,*], Wei Yuan[a], Haizhu Sun[a,*], Bai Yang[c,*]

[a] College of Chemistry, National & Local United Engineering Laboratory for Power Batteries, Northeast Normal University, Changchun 130024, China
[b] College of Material and Chemical Engineering, Chuzhou University, Chuzhou 239000, China
[c] State Key Laboratory of Supramolecular Structure and Materials, College of Chemistry, Jilin University, Changchun 130012, China

ARTICLE INFO

Article history:
Received 10 July 2019
Received in revised form 5 August 2019
Accepted 15 August 2019
Available online 16 August 2019

Keywords:
Aqueous-processed
Polymer
Nanocrystal
Recombination
Leakage current

ABSTRACT

As one of the most environmentally friendly photovoltaic (PV) conversion equipments, aqueous-processed CdTe nanocrystal solar cells (NC SCs) have attracted great interest in recent years because of their excellent properties such as high charge-carrier mobility and broad absorption. However, two issues including interfacial recombination and leakage current seriously restrict their performance. In this paper, insulating polymer poly(vinyl pyrrolidone) (PVP) is introduced into CdTe NC SCs to solve the problems. The experimental results of transmission electron microscopy (TEM), atomic force microscopy (AFM) and dark current measurements, *etc*., demonstrate the leakage current is effectively suppressed by introducing PVP. Through further designing device structure, the reduction of interfacial recombination after introducing PVP is confirmed. By strategically taking the advantages of PVP properties (*e.g*., water solubility and thermostability), the power conversion efficiency of the devices with PVP is enhanced by almost 37% compared to pure CdTe devices. This work demonstrates an effective and low-cost method to fabricate NC SCs *via* aqueous route. Moreover, it also proves that appropriate content of insulating polymer is of beneficial in promoting the PV performance.

Aqueous-processed solar cells (ASCs) have attracted great interest in recent years because of their excellent properties such as low-cost fabrication, easy processing and the unique environmentally friendly characteristics [1–7]. Varieties of water-soluble materials such as polythiophene derivatives, fullerene derivatives, CdSe, $CuInS_2$ and CdTe have been applied to solar cells [8–12]. Especially, Te based photovoltaic (PV) devices have drawn extensive attention due to their excellent charge-carrier mobility and broad absorption [13–21]. In 2014, Yang and co-workers developed the aqueous-processed nanocrystal solar cells (NC SCs) with water-soluble CdTe nanocrystals (NCs), and achieved power conversion efficiency (PCE) of 3.98% through high temperature annealing [22]. However, this efficiency is much lower than other kind of PV devices such as peroveskite SCs, polymer SCs and quantum dot SCs [23–27]. Therefore, addressing the issues in ASCs is of urgency in order to further promoting their performance.

One of the problems needs to be solved is the carrier recombination especially the interfacial recombination in PV devices [28]. In the system of CdTe NC SCs, MoO_3 is normally used as hole transport layer. This will lead to the direct contact between CdTe NCs and MoO_3, which is adverse to the PV performance because of the interfacial recombination [29]. It has been demonstrated that the tunneling layer can suppress the charge recombination at interfacial contacts to improve the device performance [30]. For example, Chandiran and co-workers utilized gallium oxide as a tunneling layer to successfully reduce electron recombination in dye-sensitized solar cells, increasing their overall efficiency [31]. Moreover, the inserted insulating layer can selectively transport one type of carriers while block another type of carriers, spatially separating photogenerated electrons and holes to limit their recombination [32]. Therefore, it is important to choose appropriate materials to work as insulating layer in order to effectively suppress the interfacial recombination and simultaneously enhance the PV performance.

In addition, pinholes and voids, which lead to the penetration of the evaporated electrode materials, often exist in the sintered NC SCs. These may result in the direct contact between the cathode and anode, leading to the generation of leakage current [33]. As a

* Corresponding authors.
E-mail addresses: ganjinchem@163.com (G. Jin), sunhz335@nenu.edu.cn (H. Sun), byangchem@jlu.edu.cn (B. Yang).
[1] These authors contributed equally to this work.

https://doi.org/10.1016/j.cclet.2019.08.024
1001-8417/

consequence, the short circuit current (J_{sc}), open-circuit voltage (V_{oc}) and fill factor (FF) will be seriously limited. Therefore, reducing the leakage current of NC SCs is another urgent and significant issue to be addressed. It is reported that multilayer processing is an effective way to reduce leakage current by interlamellar coverage [22]. However, this method is limited by the confined thickness of the fabricated film due to the limited transport distance of the carriers [34]. An alternative approach is to fill in the pinholes and voids by flexible polymers. The selected polymer will prevent the penetration of the evaporated electrode materials, thereby effectively decreasing the leakage current.

In this paper, thermostable insulating polymer poly(vinyl pyrrolidone) (PVP) was chosen to fabricate the solar cells based on CdTe NCs. As an environmentally friendly polymer, PVP has been widely used in various fields because of its advantages such as excellent water solubility, film-forming property, thermostability and low cost, *etc.* Here, the function of PVP was confirmed not only to suppress the interfacial recombination between CdTe and MoO_3, but also to decrease the leakage current, improving the device performance. Moreover, through systematically controlling thickness of the film, it was found that serious leakage current existed in thin film devices. Therefore, more PVP content was needed in thin film devices and less PVP content was used in thick film devices. As a result, PCE of 4.60% with V_{oc} of 0.52 V, J_{sc} of 17.35 mA/cm^2 and FF of 47.62% were obtained under AM1.5 G illumination, which was superior to the corresponding pure CdTe NC devices.

Because the PV devices undergo high temperature annealing during fabrication, the selected polymer needs to have good thermostability. Therefore, TGA measurement was carried out to characterize the thermostability of PVP. From the TGA curve of the pure PVP measured at 315 °C for 1.5 h (Fig. 1a), no obvious decomposition is observed for PVP after annealing for 30 min (the longest time of annealing during the fabrication of devices), and the negligible weight loss may be resulted from the desorption of moisture and impurities adsorbed on PVP itself. The wide peak located at 3470 cm^{-1} in the FT-IR spectra of PVP before and after annealing is the stretching vibration of hydroxyl group (−OH), and the strongly peak located at 1672 cm^{-1} presents the vibration of carbonyl group (C=O) (Fig. 1c). Considering that no hydroxyl group is included in the molecule structure of PVP, the existence of −OH may be resulted from the existence of enol structure in PVP. Moreover, the stretching vibration and bending vibration of C–H and the stretching vibration of C–N are clearly observed at 2940, 1416 and 1280 cm^{-1}, respectively. It is found that the position, shape and the relative intensity of absorption peak have not changed much after annealing, which is consistent with the standard FT-IR spectrum of PVP (Fig. S1 in Supporting information). The ^{1}H NMR spectra of PVP before and after annealing are shown in Fig. 1b. The peak positions of PVP are completely consistent with those of annealed PVP, confirming the good thermostability of PVP.

In addition, the hydrophilicity of the PVP film before and after annealing was slightly different detected by the contact angle measurement. As shown in Fig. S2 (Supporting information), the PVP film shows a hydrophilic surface with a contact angle of 15°, and this angle increases to 20° after annealing. These results confirm that PVP possess good thermostability which guarantees the blocking of the holes and cracks among CdTe NCs, namely, PVP can be used to prevent the penetration of the evaporated electrode materials.

In order to exclude the chemical reaction between CdTe and PVP or the changes of CdTe crystalline form, grain size and charge-carrier mobility after introducing PVP, XPS, XRD and charge-carriers mobility are tested for annealed CdTe and PVP:CdTe, respectively. XPS analysis is used to characterize the valence states of the elements in the CdTe and PVP:CdTe films. Four elements including Cd 3d, Te 3d, N 1s and S 2p are measured and the results are shown in Fig. 2. The valence states between identical elements are almost the same, which indicates that no chemical reaction occurs between CdTe and PVP.

The XRD patterns of CdTe NCs and PVP:CdTe films after annealing are presented in Fig. 3a. The peaks at 23.92°, 39.59° and 46.86° are assigned to the (111), (220) and (311) lattice planes of CdTe NCs. The consistent peak position indicates that introduction of PVP will not change the crystalline form of CdTe. By using the Scherrer formula (eq. 1):

$$D = K\lambda/\beta\cos\theta \quad (1)$$

where D is the average thickness of the crystalline grains perpendicular to the crystal plane direction, K is the Scherrer constant (0.89), β is the half width of the diffraction peak (both are 0.7°, without considering the instrumental broadening), θ is the Bragg diffraction angle (both are 11.96°), and λ is the X-ray wavelength (0.154056 nm). Both of the grain size calculated from (111) lattice plane is 11.2 nm, matches well with the statistic results (Figs. S4a and b in Supporting information) from the TEM graph (Fig. 4 and Fig. S5 in Supporting information). The same grain size

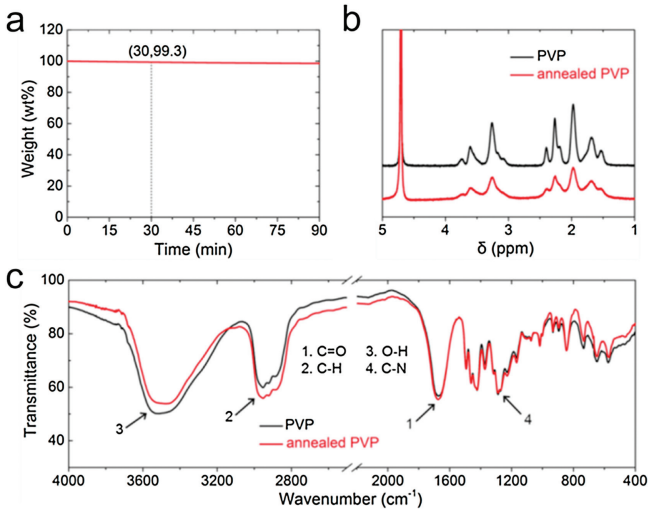

Fig. 1. (a) TGA curve of PVP measured at 315 °C for 1.5 h. The numbers in bracket represent that 99.3% of initial PVP is retained after heating 30 min at 315 °C. (b) ^{1}H NMR spectra of PVP and annealed PVP. (c) FT-IR spectra of PVP and annealed PVP.

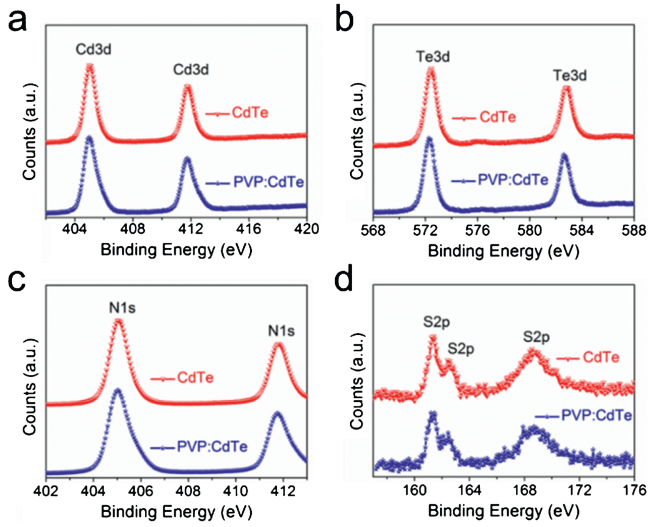

Fig. 2. XPS spectra of Cd 3d, Te 3d, N 1s and S 2p in CdTe and PVP:CdTe films.

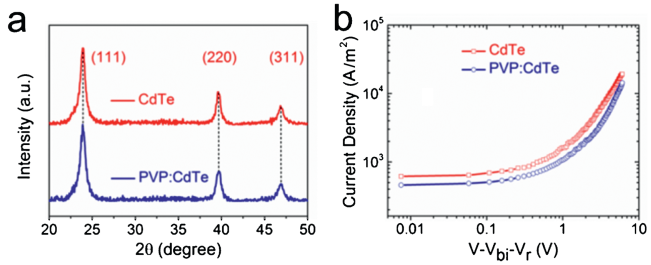

Fig. 3. (a) XRD patterns of annealed CdTe with and without PVP. (b) Charge-carrier mobility of CdTe and PVP:CdTe.

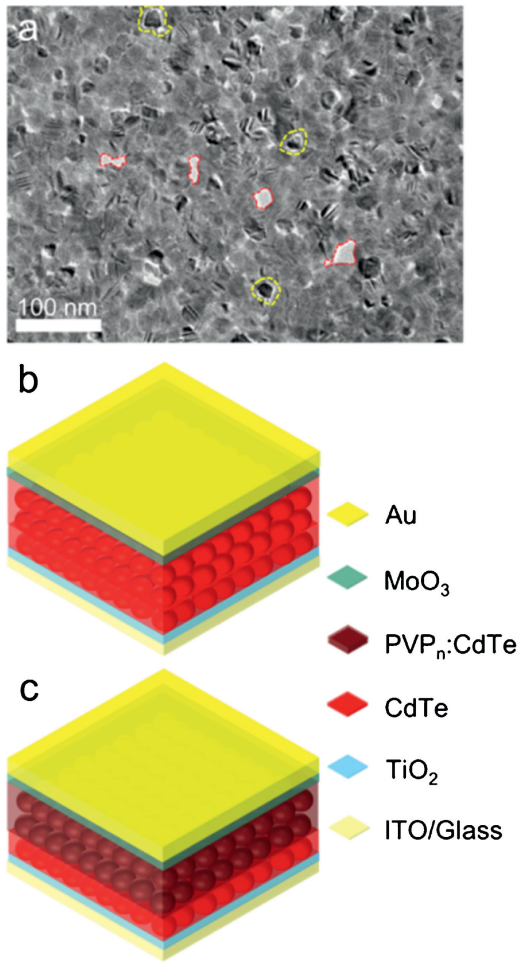

Fig. 4. (a) TEM image of the CdTe NCs film after annealing for 30 min at 315 °C, indicating the existence of pinholes and voids. Device structure of (b) CdTe (c) CdTe/PVP_n:CdTe.

indicates that introduction of PVP does not change the size of CdTe NCs. Fig. 3b exhibits the electron mobility of CdTe and PVP:CdTe through space-charge-limited-current (SCLC) method. The electron-only device structure is ITO/TiO_2/CdTe (or PVP:CdTe)/Al. The electron mobility is calculated according to the Mott-Gurney equation (eq. 2):

$$J = 9\varepsilon_0\varepsilon_r\mu(V - V_{bi} - V_r)^2/8L^3 \quad (2)$$

where ε_0 is the permittivity of free space (8.85×10^{-12} F/m), ε_r is the dielectric constant of CdTe (10), μ is the hole mobility, V is the applied voltage, V_r is the voltage drop due to contact resistance and series resistance across the electrodes, V_{bi} is the built-in voltage, and L is the film thickness (140 nm). The calculated electron mobility of CdTe and PVP:CdTe are 1.50×10^{-4} cm^2 V^{-1} s^{-1} and 1.08×10^{-4} cm^2 V^{-1} s^{-1}, respectively. The comparable mobility of CdTe and PVP:CdTe implies that introducing trace of PVP will not affect the electron mobility of CdTe. These three measurements demonstrate that no influences including chemical reaction, crystalline form, grain size and charge-carrier mobility generated after introducing PVP.

The morphology of annealed CdTe NCs thin-film is studied by TEM. The TEM image of the CdTe NCs film after annealing is shown in Fig. 4a, which clearlyproves the existence of voids among spherical NCs. The red and the yellow dotted lines represent the holes and cracks among spherical NCs in the TEM image, respectively. These holes and cracks will undoubtedly lead to the generation of leakage current. Figs. 4b and c show the fabricated devices structure, in which TiO_2 and MoO_3 are selected as electron and hole transport layer, respectively. The active layers are processed by spin-coating method. The active layers are pure CdTe (Fig. 4b), and PVP_n:CdTe/CdTe (Fig. 4c), respectively, where n represents the concentration of PVP solution. The *J–V* curves of devices with different PVP concentration are presented in Fig. S4 (Supporting information) and the detailed PV parameters are included in Table S1 (Supporting information). It is observed that the device with PVP concentration of 0.5% reaches the highest PCE of 4.60%, which is much higher than that of the pure CdTe NC SCs (3.36%), increasing about 37%. Thebest results for *J–V* curves of the pure CdTe and PVP_n:CdTe/CdTe devices are given in Fig. 5a. The three parameters including V_{oc}, J_{sc} and FF, which are summarized in Table 1, are largely enhanced. One of the reasons for the improvement of the PV performance mainly results from the reduction of leakage current. This point is confirmed through the dark current measurement shown in Fig. 5b. The pure CdTe NCs device displays a high dark current in the reverse direction while this region is distinctly suppressed in PVP:CdTe device.

The TEM graph shown in Fig. S5 presents the PVP:CdTe film after annealing. Because the contrast of organic materials is inferior to that of inorganic materials, and the quantity of PVP is too little, it is difficult to clearly observe PVP. Tapping mode AFM is employed to characterize the surface morphology of the pure CdTe and the PVP:CdTe films, which further confirms the blocking of the voids. Figs. 6a and b present the height image (5 μm × 5 μm) of the pure CdTe and the PVP:CdTe films. Figs. 6c and d show the section located at lines in Figs. 6a and b. The values of root-mean-square (RMS) roughness are 4.083 and 3.181 nm, respectively, showing that the surface of the film becomes smoother after the addition of PVP. These results strongly demonstrate that PVP successfully fill in the voids. Meanwhile, it is found that the effect of PVP on suppressing the leakage current is more significant when fabricating thin-layer devices (Figs. S6a and b in Supporting information). The devices performance for PVP concentrations of 1% is the optimum. The details are summarized in Table S2 (Supporting information). It is found that the content of PVP required in the thick-layer devices is reduced compared to the thin-layer ones. This is because that the overlap of the thick-layer

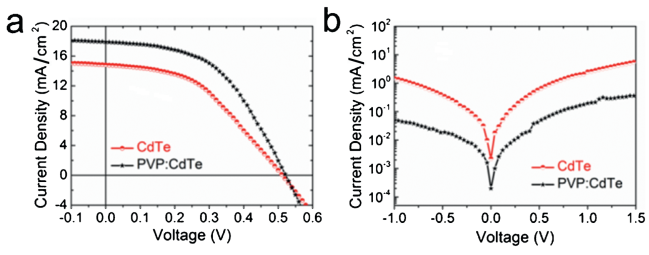

Fig. 5. (a) *J–V* curves of CdTe and PVP:CdTe devices. (b) *J–V* curves of CdTe and PVP:CdTe devices under dark condition.

Table 1
The parameters of the pure CdTe and PVP:CdTe bilayer devices with champion performance. Values in brackets are the averages, at least 6 devices are tested to obtain the averages.

Devices	V_{oc} (V)	J_{sc} (mA/cm^2)	FF (%)	PCE (%)
CdTe	0.497 [0.496]	14.9 [14.7]	45.5 [44.7]	3.36 [3.26]
PVP:CdTe	0.520 [0.517]	17.8 [17.4]	49.5 [47.6]	4.60 [4.27]

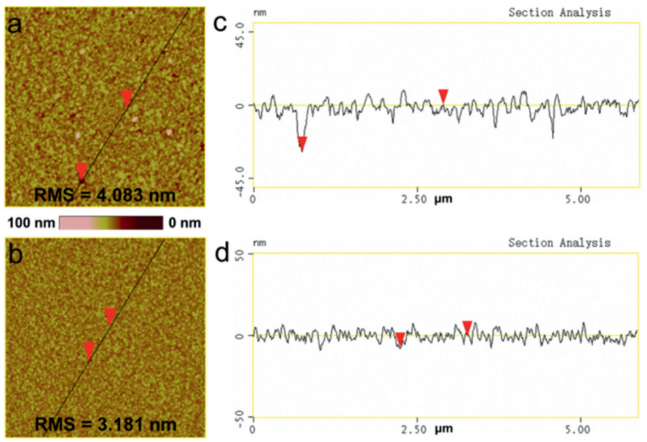

Fig. 6. AFM (size: 5 μm × 5 μm) height images of (a) CdTe, (b) PVP:CdTe and (c, d) corresponding sections located at oblique line.

CdTe NCs can also suppress the leakage current. Dark current measurement is carried out to detect the leakage current of thin-layer CdTe NCs, thick-layer CdTe NCs and PVP:CdTe devices (Fig. S6c in Supporting information). The thin-layer CdTe NCs device displays the highest dark current in the reverse direction while this region is also distinctly suppressed in the thick-layer CdTe NCs device. Moreover, the PVP:CdTe device exhibits the lowest dark current in the same range. Therefore, the leakage current is effectively reduced by the combination of multilayer processing and employing of PVP.

Furthermore, we fabricated devices with thicker active layer and the *J*–*V* curves are depicted in Fig. S7 (Supporting information). The PCE of the pure CdTe device and the PVP:CdTe device are 3.51% and 2.97%, respectively (Table S5 in Supporting information). This result demonstrates that although the devices fabricated by multilayer spin-coating can suppress leakage current, the charge-carrier transport distance is limited, and the probability of the carrier recombination will increase for the device with thicker active layer.

It is worth noting that the J_{sc} of $PVP_{0.5\%}$:CdTe device is higher than that of others devices (Tables S1 and S2). Considering that the PVP aqueous solution has a viscosity, which means that introducing PVP maybe increase the thickness of the film. Therefore, the thickness of the CdTe and $PVP_{0.5\%}$:CdTe devices are detected by the Ambios Tech. XP-2 profilometer which shows the results are about 140 nm (CdTe) and 160 nm ($PVP_{0.5\%}$:CdTe), respectively. Therefore, pure CdTe device with thickness of 160 nm is fabricated and the *J*–*V* curves of CdTe (140 nm), CdTe (160 nm) and $PVP_{0.5\%}$:CdTe (160 nm) are shown in Fig. S7. It is found that the performance of $PVP_{0.5\%}$:CdTe devices still wins the champion and the V_{oc}, FF and J_{sc} are largely improved. The details are shown in Table S3 (Supporting information). The increase for the J_{sc} and FF were about 11.3% and 9.51%, respectively, which showed similar improvement. For the V_{oc}, it is mainly determined by the difference of energy levels. Because the introduction of PVP has little influence on the energy levels of CdTe, V_{oc} show less change in comparison of J_{sc} and FF. The series resistance (R_s) and shunt resistance (R_{sh}) of the CdTe (160 nm) device are measured to be 225.3 and 4444.3 Ω cm^2, and the corresponding parameters of PVP:CdTe (160 nm) device are 149.6 and 7509.5 Ω cm^2, respectively. Apparently, the PVP:CdTe device has a tremendous improvement in the R_{sh}, indicating that the carrier recombination is significantly suppressed. This is beneficial to the increase of V_{oc} and FF.

Through measuring the absorption spectra of CdTe and PVP:CdTe after annealing (with the same film thickness) (Fig. 7a), it is discovered that the absorption value of PVP:CdTe is basically consistent with the pure CdTe. The inset shows the absorption spectra of PVP before and after annealing. The annealed PVP has a weak absorption before 250 nm, indicating that the contribution of CdTe to electric current is unaffected by PVP (measurement range of EQE is 300∼900 nm). EQE curves of CdTe and PVP:CdTe with the thickness of 160 nm are shown in Fig. 7b. Obviously, the EQE values in PVP:CdTe devices corresponding to all wavelengths are higher than those of the pure CdTe, and the integral current density are 16.1 and 17.4 mA/cm^2, respectively, which matches well with the *J*–*V* results. More importantly, thermostability PVP effectively reduces the surface contact area between CdTe and MoO_3, suppressing interfacial carrier recombination. In order to prove this point, an insulating layer of PVP is inserted between CdTe and MoO_3. Fig. 7c shows the *J*–*V* curves of the devices with and without PVP insulation layer. It is observed that the device with PVP insulation layer reaches a better performance (Table S4 in Supporting information), confirming that introduction of PVP reduces interfacial recombination of CdTe (160 nm) and PVP:CdTe (160 nm) devices. Scheme 1 is

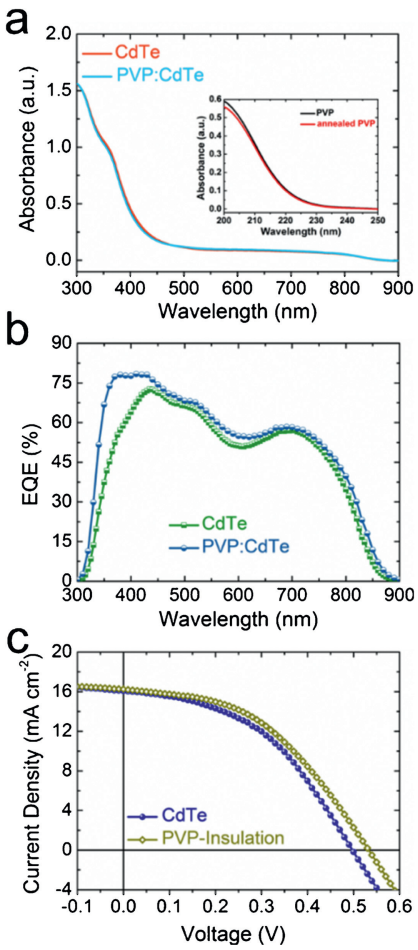

Fig. 7. (a) UV–vis-NIR absorption spectra of CdTe and PVP:CdTe active-layer and the inset is the absorption spectra of PVP (black), annealed PVP (red). (b) EQE curves of CdTe (160 nm) and PVP:CdTe (160 nm) devices. (c) *J*–*V* curves of ITO/TiO_2/CdTe/CdTe/MoO_3/Au and ITO/TiO_2/CdTe/CdTe/PVP/MoO_3/Au devices.

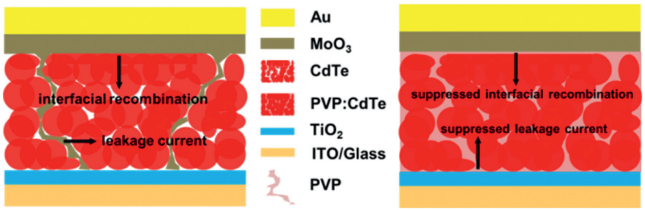

Scheme 1. Illustration of the function of PVP. The holes and cracks can be filled in by ductile polymer PVP, and the interfacial contact between CdTe and MoO_3 is also reduced after employing PVP.

drawn to visually illustrate that the function of thermostable PVP is not only to fill the voids among CdTe NCs for reduced leakage current but also decrease the surface contact area between CdTe NCs and MoO_3, which suppresses interfacial recombination and improve the overall performance of the device.

In summary, water-soluble polymer PVP was introduced into aqueous CdTe NCs for fabricating the PV devices. The blending of PVP with CdTe NCs significantly increased the device performance. By utilizing the water solubility and thermostability of PVP, the leakage current of devices was successfully reduced by filling in the voids. The reduced surface contact area between CdTe and MoO_3 guaranteed efficient suppression of interfacial recombination. Finally, PCE of 4.60% was achieved in PVP:CdTe devices and the R_{sh}, FF and V_{oc} were largely enhanced. This work makes a profound investigation on the influence of carrier recombination and leakage current in PV devices and simultaneously provides a simple, environmentally friendly and cost-effective way to achieve higher PV performance.

Acknowledgments

This work was financially supported by the National Natural Science Foundation of China (NSFC, Nos. 21574018, 51433003), and the Fundamental Research Funds for the Central Universities (No. 2412019ZD002).

Appendix A. Supplementary data

Supplementary material related to this article can be found, in the online version, at doi:https://doi.org/10.1016/j.cclet.2019.08.024.

References

[1] L. Nian, Z. Chen, S. Herbst, et al., Adv. Mater. 28 (2016) 7521–7526.
[2] D.A. Barkhouse, R. Debnath, I.J. Kramer, et al., Adv. Mater. 23 (2011) 3134–3138.
[3] S. Lu, W. Ma, G. Jin, et al., Sci. China Chem. 61 (2018) 437–443.
[4] S. Yao, L. Liu, S. Jiang, et al., RSC Adv. 8 (2018) 38591–38597.
[5] M. Lanzi, E. Salatelli, L. Giorgini, M. Marinelli, F. Pierini, Polymer 149 (2018) 273–285.
[6] L. Wang, N. Chen, G. Jin, et al., Small 14 (2018) 1803072.
[7] X. Du, Z. Chen, Z. Li, et al., Adv. Energy Mater. 4 (2014) 1400135.
[8] Q. Dong, W. Yu, Z. Li, et al., Sol. Energy Mater. Sol. Cells 104 (2012) 75–80.
[9] S. Ulum, N. Holmes, M. Barr, et al., Nano Energy 2 (2013) 897–905.
[10] J. Luo, J. Sun, P.C. Guo, et al., Mater. Lett. 215 (2018) 176–178.
[11] X. Hu, Q. Zhang, X. Huang, et al., J. Mater. Chem. 21 (2011) 15903–15905.
[12] Z. Chen, X. Du, Q. Zeng, B. Yang, Mater. Chem. Front. 1 (2017) 1502–1513.
[13] Z. Chen, H. Zhang, X. Du, et al., Energy Environ. Sci. 6 (2013) 1597–1603.
[14] G. Jin, H.T. Wei, T.Y. Na, et al., ACS Appl. Mater. Interfaces 6 (2014) 8606–8612.
[15] H. Wei, G. Jin, L. Wang, et al., Adv. Mater. 26 (2014) 3655–3661.
[16] X. Du, Q. Zeng, G. Jin, et al., Small 13 (2017) 1603771.
[17] Q. Zeng, Z. Chen, F. Liu, et al., Solar RRL 1 (2017) 1600020.
[18] Q. Zeng, L. Hu, J. Cui, et al., ACS Appl. Mater. Interfaces 9 (2017) 31345–31351.
[19] G. Jin, N. Chen, Q. Zeng, et al., Adv. Energy Mater. 8 (2018) 1701966.
[20] X. Zhu, Z. Liu, G. Shi, et al., J. Mater. Sci. Technol. 33 (2017) 418–423.
[21] L. Han, H. Fang, C. Du, et al., J. Mater. Sci. Technol. 35 (2019) 703–710.
[22] Z. Chen, H. Zhang, Q. Zeng, et al., Adv. Energy Mater. 4 (2014) 1400235.
[23] G.C. Wilkes, X. Deng, J.J. Choi, M.C. Gupta, ACS Appl. Mater. Interfaces 10 (2018) 41312–41317.
[24] F. Yang, D. Hirotani, G. Kapil, et al., Angew. Chem. Int. Ed. 57 (2018) 12745–12749.
[25] H. Choi, H.B. Kim, S.J. Ko, J.Y. Kim, A.J. Heeger, Adv. Mater. 27 (2015) 892–896.
[26] Y. Wang, K. Lu, L. Han, et al., Adv. Mater. 30 (2018) 1704871.
[27] M. Yuan, M. Liu, E.H. Sargent, Nat. Energy 1 (2016) 16016.
[28] K.W. Kemp, A.J. Labelle, S.M. Thon, et al., Adv. Energy Mater. 3 (2013) 917–922.
[29] A.K. Chandiran, N. Tetreault, R. Humphry-Baker, et al., Nano Lett. 12 (2012) 3941–3947.
[30] K. Masuko, M. Shigematsu, T. Hashiguchi, et al., IEEE J. Photovolt. 4 (2014) 1433–1435.
[31] X. Liang, S. Bai, X. Wang, et al., Chem. Soc. Rev. 46 (2017) 1730–1759.
[32] Q. Wang, Q. Dong, T. Li, A. Gruverman, J. Huang, Adv. Mater. 28 (2016) 6734–6739.
[33] G. Jin, Z. Chen, C. Dong, et al., ACS Appl. Mater. Interfaces 8 (2016) 7101–7110.
[34] G. Jin, H. Wei, Z. Cheng, et al., J. Phys. Chem. C 121 (2017) 2025–2034.